Bulletin of the Seismological Society of America, Vol. 104, No. 3, pp. 1400–1409, June 2014, doi: 10.1785/0120130102

High-Frequency Attenuation in the Lake Van Region, Eastern Turkey

by Aybige Akinci, Luca Malagnini, Robert B. Herrmann, and Dogan Kalafat

Abstract We provide a complete description of the characteristics of excitation and attenuation of the ground motion in the Lake Van region (eastern Turkey) using a data set that includes three-component seismograms from the 23 October 2011 M_w 7.1 Van earthquake, as well as its aftershocks. Regional attenuation and source scaling are parameterized to describe the observed ground motions as a function of distance, frequency, and magnitude.

Peak ground velocities are measured in selected narrow frequency bands from 0.25 to 12.5 Hz; observed peaks are regressed to define a piecewise linear regional attenuation function, a set of excitation terms, and a set of site response terms. Results are modeled through random vibration theory (see Cartwright and Longuet-Higgins, 1956).

In the log–log space, the regional crustal attenuation is modeled with a bilinear geometrical spreading $g(r)$ characterized by a crossover distance at 40 km: $g(r) \propto r^{-1.0}$ fits our results at short distances ($r < 40$ km), whereas $g(r) \propto r^{-0.3}$ is better at larger distances ($40 < r < 200$ km). A frequency-dependent quality factor, $Q(f) = 100(f/f_{ref})^{0.43}$ (in which $f_{ref} = 1.0$ Hz), is coupled to the geometrical spreading.

Because of the inherent trade-off of the excitation/attenuation parameters ($\Delta\sigma$ and κ), their specific values strongly depend on the choice made for the stress drop of the smaller earthquakes. After choosing a Brune stress drop $\Delta\sigma_{Brune} = 4$ MPa at $M_w = 3.5$, we were able to define (1) an effective high frequency, distance- and magnitude-independent roll-off spectral parameter, $\kappa_{eff} = 0.03$ s and (2) a size-dependent stress-drop parameter, which increases with moment magnitude, from $\Delta\sigma_{Brune} = 4$ MPa at M_w 3.5 to $\Delta\sigma_{Brune} = 20$ MPa at M_w 7.1.

The set of parameters mentioned here may be used in order to predict the earthquake-induced ground motions expected from future earthquakes in the region surrounding Lake Van.

Introduction

Eastern Anatolia is one of the most seismically active areas of the Middle East. Tectonics in eastern Anatolia is influenced by the northward motion of the Arabian plate and its subduction beneath the Anatolian plate (Şengör and Kidd, 1979; Şengör and Yılmaz, 1981). The Anatolian plate is compressed between the Arabian plate in the south and the Eurasian plate in the north; as a result of this tectonic setting, there are east–west (EW) trending thrust faults and northwest–southeast (NW–SE) and northeast–southwest (NE–SW) trending strike-slip faults in the region. Recently, an earthquake of magnitude M_w 7.1 occurred at 01:27 p.m. local time (10:41 UTC) on 23 October 2011 in the southern part of the Lake Van, about 20 km away from the city center of Van, Turkey (Akinci and Antonioli, 2013). The earthquake caused 644 deaths and approximately 4000 injuries. Heavy damage occurred in approximately 30% of the buildings.

The Lake Van basin is located in the east Anatolian plateau. It formed in the Late Pliocene (Şaroğlu and Yılmaz, 1986) over a basement consisting of Bitlis Metamorphics, Upper Cretaceous ophiolites, and marine sediments of Tertiary age. To the south, it includes metamorphic rocks belonging to the Bitlis Massive; volcanic and volcanoclastic rocks, originating from the two volcanoes called Nemrut Süphan and Tendürek, are found to the west and to the north (Fig. 1). Lastly, Holocene deposits in the region consist mainly of alluvial fan, lacustrine, and fluvial deposits including loosely to moderately cemented gravel, sand, silt, and unconsolidated clay horizons (Selçuk and Çiftçi, 2007).

Historically, the region experienced a large number of devastating earthquakes. In instrumental times, a large number of damaging earthquakes have occurred: 1903 Malazgirt (M_s 6.3), 1941 Erciş (M_s 5.9), 1965 Ercis (M_s 5.3), 1966 Varto (M_s 6.8), 1975 Lice (M_s 6.6), and 1976 Çaldıran (M_s 7.3). Although the Çaldıran (M_s 7.3) earthquake had a strike-slip mechanism, the Varto and Lice earthquakes exhibited thrust faulting. The 1976 Çaldıran (M_s 7.3) earthquake

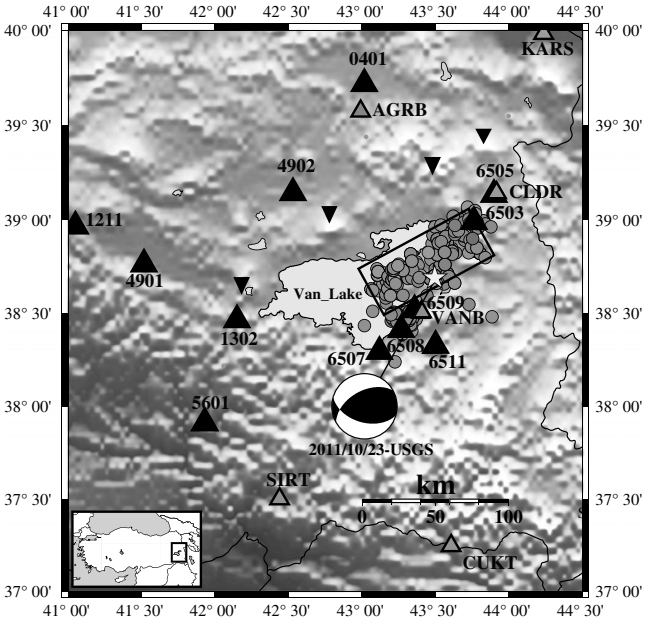

Figure 1. Regional topographic map of the study region. The circles indicate the epicentral locations of the earthquakes that are used for the regression analysis. The black and gray triangles present the locations of the Disaster and Emergency Management Presidency (AFAD) strong motion and Kandilli Observatory and Earthquake Research Institute (KOERI) broadband stations, respectively. Inverted black triangles present the volcanos. The inset shows the location of the study site.

also induced some discussion on the continuity of north Anatolian fault zone to the east of Lake Van and on its extension toward Iran. Two moderate, thrust-fault earthquakes occurred in the eastern part of Van Lake: M_w 5.4 on 14 June 1988 and M_w 5.7 on 15 November 2000.

In order to predict earthquake-induced ground motions in the area, we need to quantify the attenuation of seismic waves, the characteristics of earthquake source scaling in the region, and the spectral response of the recording sites. This characterization is required in order to assess the seismic hazard in a region. From the point of view of earthquake engineering, these parameters may be used to update the existing building codes for the new structures and/or for the retrofit of the existing ones.

In this study, we characterize the high-frequency ground motions induced by earthquakes in the Lake Van region using a set of three-component recordings from broadband seismic stations and strong-motion recordings. Instruments of the National Seismic Network are operated by Kandilli Observatory and Earthquake Research Institute (KOERI) and Afet ve Acil Durum Yönetimi Başkanlığı (Disaster and Emergency Management Presidency of Turkey, AFAD). We regress the peak values of narrow band-pass-filtered ground velocity time histories at a set of frequencies in order to define (1) an attenuation function made of a piecewise linear geometrical spreading (in the log–log space), (2) a frequency-dependent crustal $Q(f)$, and (3) an excitation function containing the competing effects of the effective stress parameter $\Delta\sigma$ and the high-frequency attenuation term $\exp(-\pi\kappa_0 f)$.

Data Set

We used 14 stations belonging to the National Strong Ground Motion Network operated by AFAD and 4 broadband stations belonging to KOERI that recorded the 23 October 2011 M_w 7.1 Van earthquake and its aftershocks between 23 October 2011 and 25 February 2012.

The AFAD strong-motion stations are equipped with CMG-5TD digital accelerometers; two of them, stations 4902 and 6503, are SIG SM-2 types. Eleven stations of ISMN are equipped by Kinemetrics SSA-2 digital accelerometers. The SIG SM-2 is a triaxial acceleration sensor with 72 dB sensitivity, coupled with a 12-bit digital converter with solid-state memory. It has a one-pole passive high-pass filter at 0.2 Hz and Butterworth antialiasing filter at 30.0 Hz. The KOERI broadband stations are equipped with Güralp CMG-40s broadband seismometers with a flat velocity response between 0.05 and 20 Hz and with a Nyquist frequency of 25 Hz.

The regression analysis was performed over 405 waveforms from earthquakes ranging in magnitude between M_L 2.4 and 6.7. The locations of the seismic stations and of selected events at epicentral distances between 5 and 200 km are shown in Figure 1. Figure 2 shows the distribution of the resulting waveforms at each station as a function of hypocentral distance (in the range between 5 and 200 km) and the number of observations as a function of magnitude.

Data Processing

A procedure introduced by Raoof *et al.* (1999) and Malagnini, Herrmann, and Di Bona (2000) is used for the analysis. This technique has been successfully applied to various regions of the world. For example, it has been used in the Apennines (Malagnini and Herrmann, 2000; Malagnini, Herrmann, and Di Bona, 2000; Malagnini *et al.*, 2008, 2011), the San Francisco Bay area (Malagnini *et al.*, 2007), the northeastern Alps (Malagnini *et al.*, 2002), the Kachchh Basin, India, region (Bodin *et al.*, 2004), the Erzincan and Marmara regions of Turkey (Akinci *et al.*, 2001, 2006), the northwestern Alps (Morasca *et al.*, 2006), eastern Sicily (Scognamiglio *et al.*, 2005), Switzerland (Bay *et al.*, 2003), central Europe (Malagnini, Herrmann, and Koch, 2000), southern California (Raoof *et al.*, 1999), Israel (Meirova *et al.*, 2008), Taiwan (D'Amico *et al.*, 2012), and western Anatolia (Akinci *et al.*, 2013). These studies demonstrated that the amplitude–distance relationships are significantly different from region to region, even at short distances from the source. Regression results can be used for the prediction of the earthquake-induced ground motions as a function of frequency and hypocentral distance, as well as for the peak amplitudes of acceleration and velocity.

To investigate the variation of seismic-wave attenuation with frequency in the region around Lake Van, each trace is

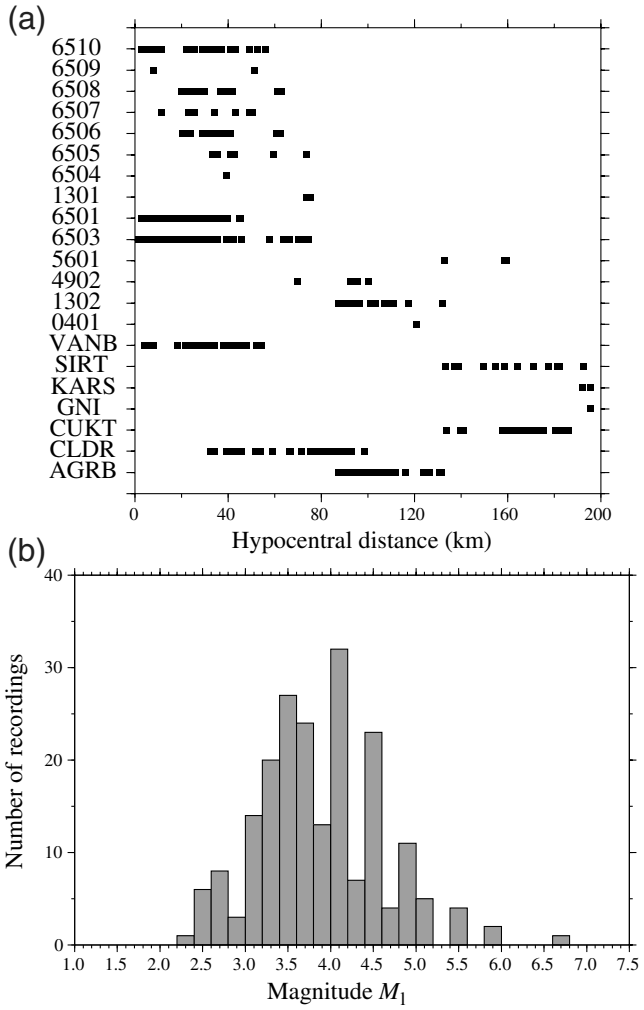

Figure 2. (a) Source–receiver hypocentral distance distribution of the data used for the regression analysis. (b) The distribution of the magnitude–number of the records used for the regression analysis.

visually inspected, and the *P* and *S* times are picked. Then each time series is band-pass filtered at 11 different center frequencies, f_c (0.25, 0.60, 0.80, 1.25, 1.75, 2.5, 3.5, 5.0, 7.0, 9.0, and 12.5 Hz). A band-pass filter at every f_c is built as the contribution of two 8-pole Butterworth filters: a low-pass filter and a high-pass filter with corner frequencies at $\sqrt{2}f_c$ and $1/\sqrt{2}f_c$, respectively. The narrowband combination of Butterworth filters used here yields a filtered signal with frequency content close to the center frequency of the filter.

Regressions are carried out on the time domain band-pass filtered peak ground velocities, such that $A_{ij}(f_c, r_{ij}) = \log_{10}\{\text{peak}[a(f_c, r_{ij})]\}$, in which peak $[a(f_c, r_{ij})]$ is the peak value of the filtered version of the seismogram recorded at the *j*th site, during the *i*th event; f_c is the specific central frequency. Data are cast in matrix form at each sampling frequency. The matrix form follows from the following scheme:

$$A_{ij}(f_c, r_{ij}) = \text{EXC}_i(f_c, r_{\text{ref}}) + \text{SITE}_j(f_c) + D(r_{ij}, r_{\text{ref}}, f_c), \quad (1)$$

in which r_{ij} is the hypocentral distance between the *i*th source (the corresponding term in the regressions would be $\text{EXC}_i(f_c, r_{\text{ref}})$) and the *j*th site term ($\text{SITE}_j(f_c)$ would be the corresponding term in the regressions). $D(r_{ij}, r_{\text{ref}}, f_c)$ is the regional attenuation term, which includes the effects of geometrical spreading and anelastic attenuation, and r_{ref} is an arbitrary reference hypocentral distance, which is needed in order to reduce the degrees of freedom of the system and to give a physical meaning to the excitation terms (i.e., the ground motion that would be recorded at the reference hypocentral distance, r_{ref}), either by a specific site or by an average network site that is generally calculated over the rock sites of the network. In the present study, matrix (1) is used at the following set of central frequencies: 0.25, 0.4, 0.6, 0.85, 1.25, 1.75, 2.5, 3.5, 5.0, 7.0, 9.0, and 12.5 Hz.

During the regressions, the degrees of freedom of the system are reduced and stability is introduced by imposing the following constraints:

1. The propagation term is normalized to zero at a specific reference distance. We select $r_{\text{ref}} = 40$ km in order to facilitate the comparisons with the results of similar studies elsewhere in Turkey (Akinci *et al.*, 2006, 2001). This constraint is formally defined as follows:

$$D(r = r_{\text{ref}}, f_c) = 0; \qquad r_{\text{ref}} = 40 \text{ km}. \quad (2)$$

   The reference distance r_{ref} is selected to be well within the range of observed distances; it should be far enough from the source that errors in source depth do not significantly affect hypocentral distances, and yet not so far that expected supercritically reflected arrivals from the Moho do not complicate the motions at distances around r_{ref}.
2. The sum of the site terms at all the available horizontal components is forced to be zero; the average absolute site term (see Malagnini *et al.*, 2004) is mapped into the $\text{EXC}_i(f_c, r_{\text{ref}})$ term. This is the reason that this function is called an excitation of observed data rather than an absolute source term. The terms $\text{EXC}_i(f_c, r_{\text{ref}})$ represent the expected ground-motion level at r_{ref}, at the average network site.

The propagation term $D(r_{ij}, r_{\text{ref}}, f_c)$ is described as a piecewise continuous function with N_{nodes} nodes:

$$D(r, r_{\text{ref}}, f_c) = \sum_{m=1}^{N_{\text{nodes}}} L_m(r) D_m, \quad (3)$$

in which $L_m(r)$ is a linear interpolation function and D_m is the value of the attenuation function at the hypocentral distance. Nodes are set to specific distances chosen in order to (roughly) evenly sample the data set (logarithmically). A smoothing constraint is applied to the propagation term $D(r, r_{\text{ref}}, f_c)$; in the case of linearly and evenly spaced nodes, the smoothing operator defines a constraint of minimum roughness, that is, a null second derivative.

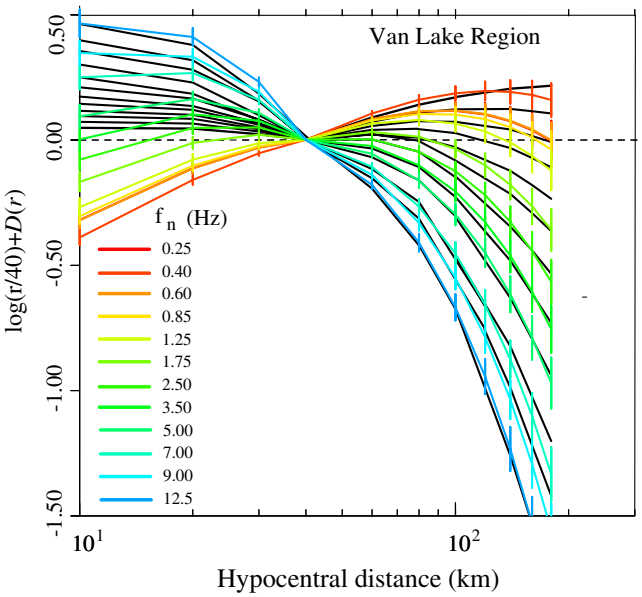

Figure 3. Empirical and regional normalized attenuation functions for the horizontal components at different frequencies that are inverted from peak-filtered amplitudes. Lines indicate empirical attenuation functions obtained from the regression of the peak-filtered velocity amplitudes at a set of frequencies. The black lines show theoretical estimates (modeled) of the same function. The color version of this figure is available only in the electronic edition.

Regressions carried out at all central frequencies yield the terms $\mathrm{EXC}_i(f_c, r_{\mathrm{ref}})$, $\mathrm{SITE}_j(f_c)$, and $D(r, r_{\mathrm{ref}}, f_c)$. An L1-norm inversion scheme is implemented for all the steps of the regressions (Bartels and Conn, 1980), so that the latter are much less sensitive to large outliers than classic least squares. Figures 3–5 present the regression results. In addition to measuring the peak value of the each filtered time series, the effective signal duration (T) was determined as the time window that encompasses the 5%–75% limits of the energy that follows the S-wave arrival (Malagnini, Herrmann, and Koch, 2000). Figure 6 presents the observed durations as a function of distance for two frequency bands. The L_1 regression curve with error bars is also shown. The measured duration will be used in modeling the results of the regressions that were carried out on the peak amplitudes.

Modeling

The purpose of the modeling is to characterize the regression results in terms of a geometrical spreading, frequency dependent $Q(f)$, source scaling, and site effects (impedance contrast and shallow attenuation) in order to be able to predict the Fourier amplitude spectra at a site. Given the spectral amplitude and the signal duration, random vibration theory (RVT; Cartwright and Longuet-Higgins, 1956) and/or stochastic time-domain simulations (Boore, 1983; Boore and Joyner, 1997) can be used to estimate the peak values of the filtered traces, but also, more importantly, other peak values such as peak accelerations, peak velocities, and response spectra. Parseval's theorem may be used for switching between the time and the frequency domains, and the convolution theorem may then be used to write the matrix form for the linear inversion (equation 1).

In summary, given a stationary, random time history of length T', RVT yields an estimate of its peak value as

$$\mathrm{Peak}[a(t)] \approx \xi a_{\mathrm{RMS}}, \tag{4}$$

in which a_{RMS} is the root mean square (rms) average of a filtered time history and is estimated in the time window of length T', which starts at the onset of S waves. The parameter $\xi = \xi(m_0, m_2, m_4)$ is a function of the specified spectral moments $[m_n = \frac{1}{\pi}\int_0^\infty \omega^n |\hat{a}(\omega)|^2 d\omega]$ of the filtered time history.

The filtering action performed by the band-pass filter makes the Fourier amplitudes different from zero only between the two-corner frequencies, allowing the following equation:

$$a_{\mathrm{RMS}}(f_i) = \sqrt{\frac{\int_0^T a^2(t, f_i)dt}{T}} = \sqrt{\frac{\int_{f_{1i}}^{f_{2i}} \hat{a}^2(f)df}{T}}. \tag{5}$$

In our study, RVT is applied to a filtered time history that is significantly different from zero only between $t = 0$ (i.e., the S-wave arrival time) and $t = T$ (i.e., the duration of the signal that follows the direct S waves). The effective duration of the ground motion (T) is calculated for each filtered seismogram, as mentioned previously.

The modeling steps are described in Malagnini *et al.* (2002). First, the $D(r)$ is modeled by defining the geometrical spreading $Q(f) = Q_0(f/f_{\mathrm{ref}})$, as well as the frequency- and distance-dependent duration for a representative earthquake size typical of the majority of observations ($f_{\mathrm{ref}} = 1.0$ Hz keeps the nondimensional nature of the attenuation parameter). The duration used for modeling the observed peak values at a given frequency, distance, and magnitude ($T(f_c, r, M_w)$) takes into account the source duration, as well as the specific dispersion of seismic waves in the region. For the small earthquakes, the distance effect (i.e., dispersion) will be much larger than source duration. The result will be a fit to the data shown in Figure 3.

The seismic sources of our data set are modeled in terms of the Brune spectral model, with a stress parameter that is a function of the earthquake's size. Because of the constraints applied to the regressions, a high-frequency filter of the form $\langle V(f)\exp(-\pi f\kappa_0)\rangle_{\mathrm{avg}} \approx \exp(-\pi f\kappa_{\mathrm{eff}})$ is common to all stations. This term is mapped onto all excitation terms: it contains the strong attenuation experienced by seismic waves just beneath the average recording site, coupled with the average elastic site effect, and is also mapped onto the excitation terms (see the Source Excitation Spectra section). The parameter κ_{eff} needs to be adjusted to fit the excitations of Figure 4a. Finally, the modeling of the source terms of equation (1) is constrained with the aid of independent estimates of the moment magnitude of a number of calibration earthquakes.

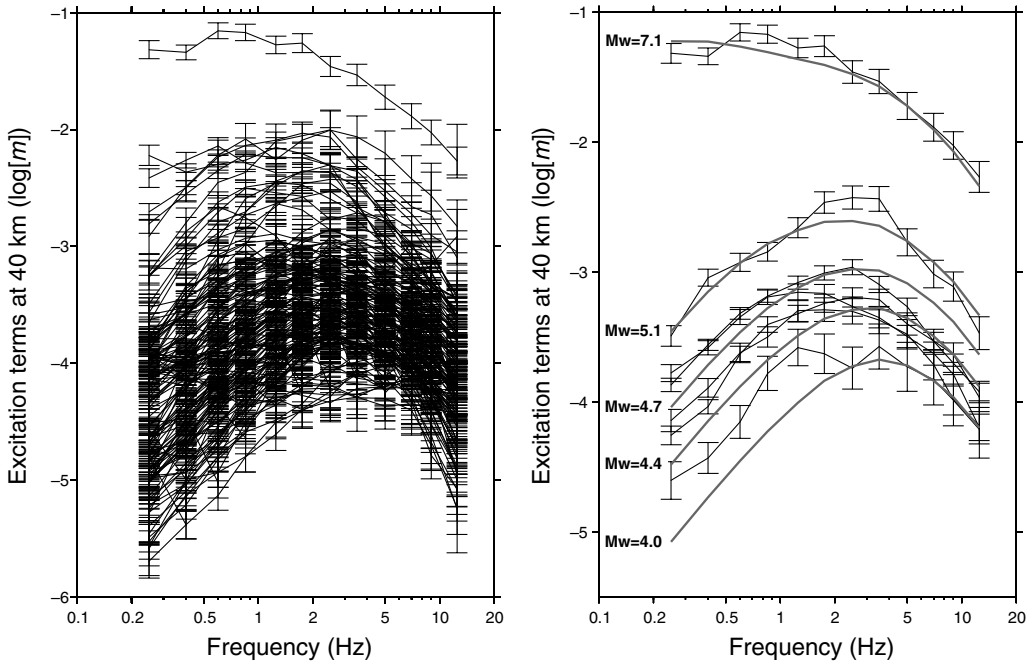

Figure 4. (a) Excitation of peak-filtered velocity at a reference hypocentral distance, $r_{ref} = 40$ km. Empirical excitation terms are for all events used in this study with magnitude between M_L 6.7 and 3.5. (b) Excitation of peak-filtered velocity at a reference hypocentral distance, $r_{ref} = 40$ km. The thin black lines present the empirical excitation terms for six moderate and large events. The gray lines present the theoretical source terms that are modeled using a single-corner (Brune, 1970) source model and the parameters obtained in this study for moment magnitudes of 4.4, 4.7, 5.0, and 7.1 (Table 1).

Attenuation Model for the Region

Figure 3 shows the results of the regressions, in terms of attenuation of peak velocity amplitudes $D(r, r_{ref}, f_c)$ plotted as a function of frequency and hypocentral distance for the Lake Van region. A search through the solution space yielded the following functional forms and parameters that describe the 0.25–12.5 Hz observations. Using $f_{ref} = 1.0$ Hz,

$$Q(f) = 100(f)^{0.43}, \tag{6}$$

with the geometrical spreading defined as the bilinear relationships

$$\begin{aligned} g(r) &= r^{-1.0} \qquad r \le r_0 = 40 \text{ km} \\ g(r) &= (1/r_0)(r_0/r)^{0.3} \qquad r > r_0. \end{aligned} \tag{7}$$

These parameters fit the $D(r)$ within the error bounds of the regression results at all distances within our sampled range. The differences between observed and predicted $D(r)$ at distance less than 20 km are not to be considered significant because of the smaller number of observations and because of the lack of precision in the hypocentral locations. The greater deviation at low frequencies and short distances may be related to the fact that, at these long periods, the filtered signal in the *S*-wave window may be affected by the presence of *P* waves. Although we did not derive uncertainties on these parameters, the uncertainty of any prediction will be on the order of the error bars resulting from the regression. For distances beyond 40 km, $g(r)$ requires $r^{-0.3}$ that is shallower than what is expected for surface waves ($r^{-0.5}$). The exponents of the geometrical spreading function describe the geometry of the wavefront (e.g., spherical or cylindrical propagation, or even characterized by the appearance of supercritical reflections in the transitional distance ranges), which strongly depends on the velocity structure of the medium (Aki and Richards, 2002). It is clear that if we fix the geometrical spreading function to $1/r$, we hypothesize a spherical wavefront and, hence implicitly, a uniform crust. Our $g(r)$ results differ from $r^{-0.5}$ at relatively long distances. This could be caused by the boundary between the fall-off of direct waves, the emergence of lower crustal or Moho reflections and the contribution of the *SmS* phases.

The attenuation parameters obtained in this study have already been validated by Akinci and Antonioli (2013) against the observed ground motions recorded during the 23 October 2011 main event of the Lake Van sequence through a dynamic corner frequency approach (Motazedian and Atkinson, 2005; Boore, 2009). The present work and related studies (the ones cited earlier and a number of recent ones, including Ugurhan *et al.*, 2012; Akinci and Antonioli, 2013; Edwards and Fäh, 2013; Rietbrock *et al.*, 2013) have shown that differences in the attenuation characteristics of the crust between areas characterized by different tectonic regimes and thermal ages may significantly impact the hazard estimates if the predictive relationships for the ground motion are computed over data sets of heterogeneous nature.

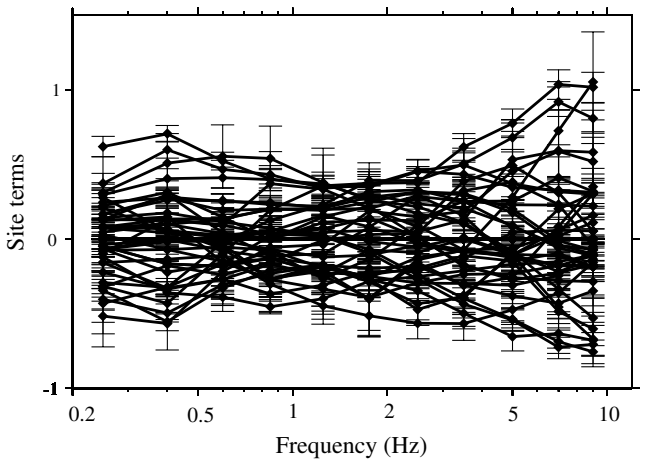

Figure 5. Horizontal-component site terms as a function of frequency inverted from the Lake Van aftershock data, with the constraint that the sum of all horizontal site terms is zero. Each line connects a separate site, with two standard-deviation error bars shown for each site at each frequency.

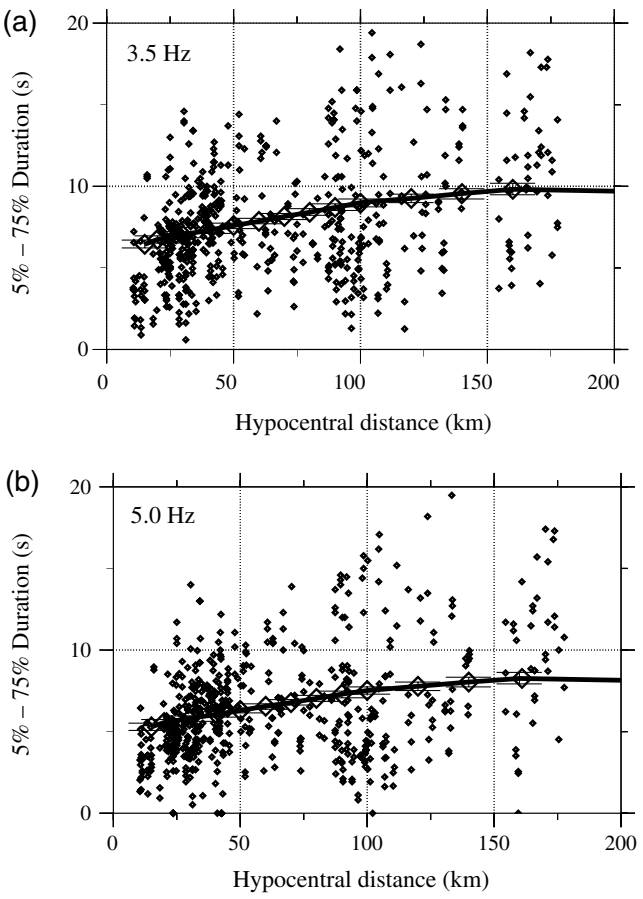

Figure 6. Distance dependence duration for (a) 3.5 Hz and (b) 5 Hz filtered data. The small dark diamonds represent the individual values of duration. Light gray diamonds indicate the values of duration computed at a set of nodes by using an inversion. Uncertainties are computed using a least squares algorithm.

Calibrating Moment Magnitudes

Using the western United States crustal model (Herrmann *et al.*, 2011), we computed seven moment tensors for the Van region. Each inversion involves 3–5 three-component broadband waveforms. In terms of the signal-to-noise ratio at very low frequency, the quality of the broadband recordings was not excellent. In Table 1, we list only the moment magnitudes of the events for which we obtained compressive mechanisms. The two listed events marked with '*' are characterized by T axes almost 90° off from that of the main event, although the synthetic amplitudes reproduce well the observed ones. The most robust parameters of the listed inversions are the seismic moments, which are used in order to check the validity of the excitation terms (see the Source Excitation Spectra section).

Source Excitation Spectra

The empirical excitation terms $\mathrm{EXC}_i(f_c, r_{\mathrm{ref}})$ in equation (1) is related to the source spectrum, and it is the expected average level of ground motion at $r = r_{\mathrm{ref}}$ for each earthquake (at the average network site). These terms may be modeled using a Brune (1970, 1971) spectral model that is propagated to the reference hypocentral distance of 40 km through the expression in the frequency domain

$$s(f, M_{\mathrm{w}})(1/r_{\mathrm{ref}}) \exp(-\pi r_{\mathrm{ref}} \beta) \times Q_0 (f/f_{\mathrm{ref}})^{\eta} \langle V(f) \exp(-\pi f \kappa_0) \rangle_{\mathrm{avg}}, \quad (8)$$

in which $V(f)$ represents the average site amplification term relative to hard rock (Atkinson and Silva, 1997). κ_0 describes the fall-off of the high-frequency motion at the site (Anderson

Table 1
Summary of Moment Tensor Solutions and Stress-Drop Parameters

Event ID	Latitude (°)	Longitude (°)	Depth (km)	Strike	Dip	Rake	M_{w}	Stress Drop MPa ($\Delta\sigma_{\mathrm{Brune}}$)	M_0 (N·m)	%Fit
20111023104120	38.6890	43.4657	11.0	240	50	85	7.08	20	5.25×10^{19}	0.54
20120120095737	38.7032	43.4975	12.0	50	45	90	4.70	9.0	1.41×10^{16}	0.62
201112112052918	38.5017	43.2308	6.0	55	75	95	3.65	4.0	3.76×10^{14}	0.40
20111203013054	38.8513	43.7850	2.0	45	55	50	4.08	4.5	1.66×10^{15}	0.34
20111117123831	38.8805	43.5815	5.0	250	65	50	3.97	4.5	1.14×10^{15}	0.55
20111108220550*	38.7060	43.1082	10.0	335	35	70	5.11	130	5.82×10^{16}	0.53
20111105191916*	38.8147	43.5147	4.0	135	40	40	4.33	6.5	3.94×10^{15}	0.64

*Southwest–northeast are not in agreement with the direction of maximum compressional stress in the region.

and Hough, 1984). The term $\langle V(f)\exp(-\pi f\kappa_0)\rangle_{\text{avg}}$ represents the average distortion induced by the network sites, so that we may use the parameter κ_{eff} in our modeling, in which $\exp(-\pi f\kappa_{\text{eff}})$ is used to approximate the term $\langle V(f)\exp(-\pi f\kappa_0)\rangle_{\text{avg}}$.

The form of $s(f, M_w)$ representing the Fourier velocity spectra is following:

$$s(f, M_w) = C[M_0 4\pi\rho\beta^3](2\pi f)S(f), \tag{9}$$

$$C = (0.55 \times 2.0 \times 0.707) = 0.24, \tag{10}$$

in which $\log M_0 = 1.5M_w + 6.03$ from Hanks and Kanamori (1979). The constant parameter C in equations (9) and (10) (Boore, 1983, 1986; Atkinson and Boore, 1995) takes the following into account:

1. the radiation pattern rms-averaged over a suitable range of azimuth and take-off angles ($\langle R\Theta\Phi\rangle$, Boore and Boatwright, 1984), 0.55;
2. the amplification due to the free surface, 2.0; and
3. the partitioning of energy into horizontal components, 0.707.

$S(f)$ is basically the single-corner (f_c) Brune crack model in a crust with density $\rho = 2.8$ g/cm^3, shear-wave velocity 3.5 km/s, and seismic moment M_0. In our excitation terms, $S(f)$ is attenuated to the reference distance of 40 km. For Brune model, the corner frequency f_c is related to stress-drop parameter following the expression

$$f_c = 0.49\beta(\Delta\sigma_{\text{Brune}}M_0)^{1/3}, \tag{11}$$

in which $\Delta\sigma_{\text{Brune}}$ is the stress-drop parameter in units of Pa. RVT is used to model the time-domain regression results by using the duration at the reference distance together with the spectral scaling.

Figure 4a,b shows the inverted excitation terms and theoretical source models obtained for the peak of the filtered amplitudes derived from RVT synthetics. Individual earthquake source excitation curves at 40 km are shown as black thin curves. The thick gray lines in Figure 4b show the predicted excitation terms obtained by using equations (9)–(11), at the moment magnitudes corresponding to those calculated for the plotted events.

It is very clear that a trade-off exists between κ_{eff} and $\Delta\sigma_{\text{Brune}}$: whereas the former governs the high-frequency decay of the theoretical excitation terms, $\Delta\sigma_{\text{Brune}}$ determines the amount of seismic energy that is radiated away from the source. The two parameters strongly compete against each other in defining the observed spectral amplitudes at high frequency, and such a trade-off cannot be solved with the approach described in this paper.

We point out that the absolute source scaling in the region should be tackled by a dedicated study, like the ones by Malagnini, Mayeda, *et al.* (2014), Malagnini, Munafò, *et al.* (2014), or Morasca *et al.* (2005). However, in order to resolve the impasse and to come up with an effective excitation model for the ground motion, we choose a stress-drop value of $\Delta\sigma_{\text{Brune}} = 4$ MPa at $M_w = 3.5$ and obtain $\kappa_{\text{eff}} = 0.03$ s by fitting the high-frequency part of the events of that size. Because κ_{eff} does not depend on the earthquake's seismic moment, but only on the average shallow attenuation properties beneath the network sites, using $\kappa_{\text{eff}} = 0.03$ s, we fitted the spectral levels of all events with the appropriate $\Delta\sigma = \Delta\sigma(M_w)$ (see Table 1).

The excitation terms of the seven events for which we have the seismic moments (Table 1) are plotted against our predictions in Figure 4b. The fit for the main earthquake ($M_w = 7.1$) is excellent for all frequencies, meaning we are confident in using this model to predict the ground motions in the region. From the visual inspection of the values listed in Table 1, we see that, for the earthquakes listed, stress drop seems to steadily increase with increasing moment magnitude: from $\Delta\sigma_{\text{Brune}} = 4$ MPa at $M_w = 3.5$, to $\Delta\sigma_{\text{Brune}} = 20$ MPa at $M_w = 7.1$.

Site Terms

Figure 5 shows the site terms from the regression on horizontal filtered peak amplitudes. Because the constraint of null average was applied to the horizontal component site terms at the sites of the broadband stations, we may interpret the excitation terms of equation (1) in terms of the horizontal ground motion that would be observed at the average network site, 40 km away from the hypocenter.

We stress that anything systematic affecting all sites (e.g., if all instruments are deployed on the same sedimentary basin) would not change the site terms of Figure 5. Instead, any systematic behavior affecting the site terms would be mapped into the excitation terms of Figure 4. There are ways to reduce or eliminate the inherent trade-off between sources and sites that comes from equation (1) (see Malagnini *et al.*, 2004, 2007), although these techniques were not applied in the present case.

Because the site terms continue to trade-off with the empirical excitation terms, they are of no practical use in the present form, exception made for the analysis of relative discrepancies in the shallow site response. The latter is very useful for the quality control of the entire data set and of the obtained results.

However, the variability seen among the individual site terms, which could be used for quantifying the uncertainties on predicted ground motions, is of some use. With respect to a regional predictive relationship for the ground motion, the best choices would be the generic site types (Boore and Joyner, 1997) that may be representative of the situations of a specific area of interest.

Comparisons with Previous Studies

The values of the attenuation parameters for the *S* waves calculated in the present study up to 10 Hz are in agreement

with those by previous studies performed in the region (Mitchell *et al.*, 1997; Mitchell and Cong, 1998; Gök *et al.*, 2000, 2003, 2007, 2008; Sandvol *et al.*, 2001; Zor *et al.*, 2007; Pasyanos *et al.*, 2009; Sertcelik, 2012). For example, Zor *et al.* (2007) developed the tomography model for *Lg* crustal attenuation within the Turkish plateau using the two-station method and backprojection tomography. They observed strong attenuation ($Q_0 = 70$–100) in the east Anatolian plateau, due to the widespread young volcanism in the region and most probably caused by intrinsic attenuation. Pasyanos *et al.* (2009) obtained similar values to those found by Zor *et al.* (2007) using a new attenuation formulation that explicitly defines the source expression in terms of seismic moment and the amplitudes of regional phases *Pn*, *Pg*, *Sn*, and *Lg* over a wide range frequency band in the Middle East. They observed that eastern Turkey has the highest attenuation over the whole frequency band. Sertcelik (2012) estimated the attenuation of coda waves $Q_c(f)$ for different lapse times and frequencies in the east Anatolia fault zone (EAFZ) using a single backscattering model of *S*-coda envelopes. They computed $Q_0 = 95$ with a frequency dependence of $\eta = 0.67$ for 40 s lapse times along the EAFZ. All of these studies indicate very high attenuation (low Q) values over the east Anatolian plateau; with a similar Q value ($\sim$100) over the rest of the region. Volcanic regions are often observed to possess low LgQ, possibly due to high attenuation of waves by partial melt in the crust. In fact, several studies indicate the presence of low-velocity zones throughout the east Anatolian plateau, that are interpreted in terms of presence of partial melt in the uppermost mantle and within the crust. Low *Pn* velocities, coupled with high *Sn* attenuation, are explained by Gök *et al.* (2003) as an indication of anomalously hot lithosphere in the study region.

Conclusions

We characterize wave propagation and source scaling for the seismic sequence of Lake Van, eastern Turkey, in the frequency range between 0.25 and 12.5 Hz and in the distance range between 10 and 150 km. Results presented in this study show strong crustal attenuation, as well as the effects of the arrivals of supercritical reflections, probably off the Moho. The latter are indicated by the change in apparent geometrical spreading occurring at a hypocentral distance of 40 km (which should be roughly twice the depth of the discontinuity off which the supercritical reflection are produced). Supercritical reflections would produce the change in slope of the geometrical spreading function occurring at the hypocentral distance of 40 km, at which $g(r)$ goes from a body-wave-like function ($g(r) = 1/r$) to a functional form ($g(r) \propto r^{-0.3}$) that is substantially shallower than what is expected for *Lg* or surface waves.

The excitation spectra of the events that entered the regressions described in this study were satisfactorily fit by using the propagation model described by equations (6) and (7), from which the empirical excitation terms were completely decoupled by constraint (2). More ingredients used for the spectral fit are a single-corner frequency Brune spectral model with an increasing stress parameter for increasing earthquake's size and a high-frequency roll-off parameter $\kappa_{\text{eff}} = 0.03$ s.

We made clear that the absolute values of our stress drops all depend on the choice mentioned earlier ($\Delta\sigma_{\text{Brune}} =$ 4 MPa at M_w 3.5), although a very different stress-drop value could not fit the spectra of the M_w 3.5 events, regardless of the parameter κ_{eff}. Our modeling effort indicates a clear trend for the stress parameter, which constantly increases for increasing magnitude. With the described choice for the parameter κ_{eff}, we obtained the following values of the Brune stress drop: $\Delta\sigma_{\text{Brune}}(M_w = 4) = 4$ MPa, $\Delta\sigma_{\text{Brune}}(M_w = 5) = 13$ MPa, whereas $\Delta\sigma_{\text{Brune}}(M_w = 7.1) = 20$ MPa best reproduced the empirical excitation spectrum of the main event (see Table 1). Our findings about the Van earthquake source scaling are in agreement with general results observed by Malagnini, Mayeda, *et al.* (2014) and Malagnini, Munafò, *et al.* (2014).

Stress drops as a function of moment magnitude, together with the parameters of the crustal attenuation, are the main ingredients to both the deterministic and the stochastic methods that may be used in order to predict the strong ground motions. Such methods are particularly important when there are not enough actual recordings to allow the assessment of the ground shaking at large magnitude, especially in the near-fault area (Edwards and Fäh, 2013; Rietbrock *et al.*, 2013).

Because of the strong differences in the crustal attenuation and in source scaling that has been pointed out in many recent papers (e.g., the ones by Malagnini and coworkers that are listed in this study), regional studies must be systematically carried out for purposes of ground-motion prediction. Finally, ground-motion studies performed over homogenous, large data sets of waveforms from large earthquake sequences recorded at local and regional distances can reduce the uncertainties of region-specific ground-motion prediction equations.

Data and Resources

Strong ground motion data were obtained from the Disaster and Emergency Management Presidency (AFAD) website (http://kyh.deprem.gov.tr; last accessed November 2011). Processed and raw strong-motion data are posted on the Middle East Technical University, Earthquake Engineering Research Center (METU–EERC) website (http://eerc.metu.edu.tr/vaneq-23102011; last accessed November 2011). Broadband data were obtained from the Kandilli Observatory and Earthquake Research Institute website (http://udim.koeri.boun.edu.tr; last accessed January 2013). Details of the location of the Van earthquake were obtained from the U. S. Geological Survey website, http://earthquake.usgs.gov/earthquakes/eqinthenews/2011/usb0006bqc/finite_fault.php (last accessed November 2011). Many of the plots were made using Generic Mapping Tools, version 4.2.1

(www.soest.hawaii.edu/gmt, last accessed December 2008; Wessel and Smith, 1998).

Acknowledgments

We would like to thank those at the Earthquake Department of the Disaster and Emergency Management Presidency (AFAD) and the Kandilli Observatory and Earthquake Research Institute (KOERI) who made the data available right after the earthquake. These recordings are the basis of our study. We thank Glenn Biasi, Rengin Gök, and Associate Editor Zhigang Peng for their suggestions, which helped us to improve the manuscript. In this study, many of the figures are prepared using Generic Mapping Tools (version 4.2.1), and the Seismic Analysis Code (SAC) software is used for many of the calculations through a set of several macros.

References

Aki, K., and P. G. Richards (2002). *Quantitative Seismology*, 2nd Edition, University Science Books, Sausalito, California, 678 pp.

Akinci, A., and A. Antonioli (2013). Observations and stochastic modeling of strong ground motions for the 2011 October 23 M_w 7.1 Van, Turkey, earthquake, *Geophys. J. Int.* **192,** no. 3.

Akinci, A., S. D'Amico, L. Malagnini, and A. Mecuri (2013). Scaling earthquake ground motions in western Anatolia, Turkey, *Phys. Chem. Earth* **63,** 124–135.

Akinci, A., L. Malagnini, R. B. Herrmann, R. Gök, and M. Sorensen (2006). Ground motion scaling in the Marmara region, Turkey, *Geophys. J. Int.* **166,** 635–651.

Akinci, A., L. Malagnini, R. B. Herrmann, N. A. Pino, L. Scognamiglio, and H. Eyidogan (2001). High-frequency ground motion in the Erzincan region, Turkey: Inferences from small earthquakes, *Bull. Seismol. Soc. Am.* **91,** 1446–1455.

Anderson, J. G., and S. E. Hough (1984). A model for the shape of the Fourier amplitude spectrum of acceleration at high frequencies, *Bull. Seismol. Soc. Am.* **74,** 1969–1993.

Atkinson, G. M., and D. M. Boore (1995). Ground-motion relations for eastern North America, *Bull. Seismol. Soc. Am.* **85,** 17–30.

Atkinson, G. M., and W. Silva (1997). An empirical study of earthquake source spectra for California earthquakes, *Bull. Seismol. Soc. Am.* **87,** 97–113.

Bartels, R., and A. Conn (1980). Linearly constrained discrete l1 problems, *ACM Trans. Math. Soft.* **6,** 594–608.

Bay, F., D. Fah, L. Malagnini, and D. Giardini (2003). Spectral shear wave ground motion scaling for Switzerland, *Bull. Seismol. Soc. Am.* **93,** 414–429.

Bodin, P., L. Malagnini, and A. Akinci (2004). Ground motion scaling in the Kachchh basin, India, deduced from after-shocks of the 2001 M_w 7.6 Bhuj earthquake, *Bull. Seismol. Soc. Am.* **94,** 818–827.

Boore, D. M. (1983). Stochastic simulation of high-frequency ground motions based on seismological models of the radiated spectra, *Bull. Seismol. Soc. Am.* **73,** 1865–1894.

Boore, D. M. (1986). Short-period *P*- and *S*-wave radiation from large earthquakes: Implications for spectral scaling relations, *Bull. Seismol. Soc. Am.* **76,** 43–64.

Boore, D. M. (2009). Comparing stochastic point-source and finite-source ground-motion simulations: SMSIM and EXSIM, *Bull. Seismol. Soc. Am.* **99,** 3202–3216.

Boore, D. M., and J. Boatwright (1984). Average body-wave radiation coefficients, *Bull. Seismol. Soc. Am.* **74,** 1615–1621.

Boore, D. M., and W. B. Joyner (1997). Site amplifications for generic rock sites, *Bull. Seismol. Soc. Am.* **87,** 327–341.

Brune, J. (1970). Tectonic stress and the spectra of seismic shear waves from earthquakes, *J. Geophys. Res.* **75,** 4997–5009.

Brune, J. (1971). Correction, *J. Geophys. Res.* **76,** 5002.

Cartwright, D. E., and M. S. Longuet-Higgins (1956). The statistical distribution of the maxima of a random function, *Proc. Roy. Soc. Lond.* **237,** 212–232.

D'Amico, S., A. Akinci, and L. Malagnini (2012). Predictions of high-frequency ground-motion in Taiwan based on weak motion data, *Geophys. J. Int.* **189,** 611–628.

Edwards, B., and D. Fäh (2013). A stochastic ground-motion model for Switzerland, *Bull. Seismol. Soc. Am.* **103,** no. 1, doi: 10.1785/0120110331.

Gök, R., H. Mahdi, H. Al-Shukri, and A. J. Rodgers (2008). Crustal structure of Iraq from receiver functions and surface wave dispersion: Implications for understanding the deformation history of the Arabian–Eurasian collision, *Geophys. J. Int.* **172,** 1179–1187.

Gök, R., M. E. Pasyanos, and E. Zor (2007). Lithospheric structure of the continent–continent collision zone: Eastern Turkey, *Geophys. J. Int.* doi: 10.1111/j.1365-246X.2006.03288.x.

Gök, R., E. Sandvol, N. Turkelli, D. Seber, and M. Barazangi (2003). Sn attenuation in the Anatolian and Iranian plateau and surrounding regions, *Geophys. Res. Lett.* **30,** no. 24, 8042, doi: 10.1029/2003GL018020.

Gök, R., N. Turkelli, E. Sandvol, D. Seber, and M. Barazangi (2000). Regional wave propagation in Turkey and surrounding regions, *Geophys. Res. Lett.* **27,** no. 3, 429–432.

Hanks, T. C., and H. Kanamori (1979). A moment magnitude scale, *J. Geophys. Res.* **84,** no. B5, 2348–2350.

Herrmann, R. B., H. Benz, and C. J. Ammon (2011). Monitoring the earthquake source process in North America, *Bull. Seismol. Soc. Am.* **101,** no. 6, 2609–2625, doi: 10.1785/0120110095.

Malagnini, L., and R. B. Herrmann (2000). Ground-motion scaling in the region of the Umbria-Marche earthquake of 1997, *Bull. Seismol. Soc. Am.* **90,** 1041–1051.

Malagnini, L., A. Akinci, R. B. Herrmann, N. A. Pino, and L. Scognamiglio (2002). Characteristics of the ground motion in northeastern Italy, *Bull. Seismol. Soc. Am.* **92,** 2186–2204.

Malagnini, L., A. Akinci, K. Mayeda, I. Munafò, R. B. Herrmann, and A. Mercuri (2011). Characterization of earthquake-induced ground motion from the L'Aquila seismic sequence of 2009, Italy, *Geophys. J. Int.* **184,** 325–337.

Malagnini, L., R. B. Herrmann, and M. Di Bona (2000). Ground-motion scaling in the Apennines (Italy), *Bull. Seismol. Soc. Am.* **90,** 1062–1081.

Malagnini, L., R. B. Hermann, and K. Koch (2000). Regional ground motion scaling in central Europe, *Bull. Seismol. Soc. Am.* **90,** 1052–1061.

Malagnini, L., K. Mayeda, A. Akinci, and P. L. Bragato (2004). Estimating absolute site effects, *Bull. Seismol. Soc. Am.* **94,** 1343–1352.

Malagnini, L., K. Mayeda, S. Nielsen, S.-H. Yoo, I. Munafò, C. Rawles, and E. Boschi (2014). Scaling transition in earthquake sources: A possible link between seismic and laboratory measurements, *Pure Appl. Geophys.* doi: 10.1007/s00024-013-0749-8.

Malagnini, L., K. Mayeda, R. Uhrhammer, A. Akinci, and R. B. Herrmann (2007). A regional ground motion excitation/attenuation model for the San Francisco region, *Bull. Seismol. Soc. Am.* **97,** no. 3, 843–862; doi: 10.1785/0120060101.

Malagnini, L., I. Munafò, M. Cocco, S. Nielsen, K. Mayeda, and E. Boschi (2014). Gradual fault weakening with seismic slip: Inferences from the seismic sequences of L'Aquila, 2009 and Northridge, 1994, *Pure Appl. Geophys.* doi: 10.1007/s00024-013-0752-0.

Malagnini, L., L. Scognamiglio, A. Mercuri, A. Akinci, and K. Mayeda (2008). Strong evidence for non-similar earthquake source scaling in central Italy, *Geophys. Res. Lett.* **35,** L17303, doi: 10.1029/2008GL034310.

Meirova, T., R. Hofstetter, Z. Ben-Avraham, D. M. Steinberg, L. Malagnini, and A. Akinci (2008). Weak-motion-based predictive relationships for the ground motion in Israel, *Geophys. J. Int.* **175,** 1127–1140, doi: 10.1111/j.1365-246X.2008.03953.x.

Morasca, P., L. Malagnini, A. Akinci, D. Spallarossa, and R. B. Herrmann (2006). Ground-motion scaling in the western Alps, *J. Seismol.* **10,** no. 3, doi: 10.1007/s10950-006-9019-x.

Morasca, P., K. Mayeda, L. Malagnini, and W. Walter (2005). Coda-derived source spectra, moment magnitudes and energy-moment scaling in the western Alps, *Geophys. J. Int.* **160,** no. 1, 263–275, doi: 10.1111/j.1365-246X.2005.02491.x.

Mitchell, B., and L. Cong (1998). *Lg* coda *Q* and its relation to the structure and evolution of continents: A global perspective, *Pure Appl. Geophys.* **153,** 655–663.

Mitchell, B. J., Y. Pan, J. Xie, and L. Cong (1997). *Lg* coda *Q* variation across Eurasia and its relation to crustal evolution, *J. Geophys. Res.* **102,** 22,767–22,779.

Motazedian, D., and G. M. Atkinson (2005). Stochastic finite-fault modeling based on a dynamic corner frequency, *Bull. Seismol. Soc. Am.* **95,** 995–1010.

Pasyanos, M. E., E. M. Matzel, W. R. Walter, and A. J. Rodgers (2009). Broadband *Lg* attenuation modeling in the Middle East, *Geophys. J. Int.* **177,** 1166–1176, doi: 10.1111/j.1365-246X.2009.04128.x.

Raoof, M., R. B. Herrmann, and L. Malagnini (1999). Attenuation and excitation of three-component ground motion in southern California, *Bull. Seismol. Soc. Am.* **89,** 888–902.

Rietbrock, A., F. Strasser, and B. Edwards (2013). A stochastic earthquake ground motion prediction model for the United Kingdom, *Bull. Seismol. Soc. Am.* **103,** no. 1, doi: 10.1785/0120110231.

Sandvol, E., K. Al-Damegh, A. Calvert, D. Seber, M. Barazangi, R. Mohamad, R. Gök, N. Turkelli, and C. Gurbuz (2001). Tomographic imaging of observed regional wave propagation in the Middle East, *Pure Appl. Geophys.* **158,** 1121–1163.

Şaroğlu, F., and Y. Yılmaz (1986). Doğu Anadolu'da neotektonik dönemdeki jeolojik evrim ve havza modelleri, *Maden Tetkik ve Arama Dergisi* **107,** 73–94 (in Turkish).

Scognamiglio, L., L. Malagnini, and A. Akinci (2005). Ground motion scaling in Eastern Sicily, *Bull. Seismol. Soc. Am.* **95,** no. 2, 568–578.

Selçuk, L., and Y. Çiftçi (2007). Microzonation of the Plio-Quaternary soils: A study on the liquefaction risk potential in the Lake Van basin, Turkey, *Bull. Eng. Geol. Environ.* **66,** 161–176.

Şengör, A. M. C., and W. S. F. Kidd (1979). Postcollisional tectonics of the Turkish-Iranian plateau and a comparison with Tibet, *Tectonophysics* **55,** 361–376.

Şengör, A. M. C., and Y. Yılmaz (1981). Tethyan evolution of Turkey: A plate tectonic approach, *Tectonophysics* **75,** 181–241.

Sertcelik, F. (2012). Estimation of coda wave attenuation in the east Anatolia fault zone, Turkey, *Pure Appl. Geophys.* **169,** no. 7, 1189–1204.

Ugurhan, B., A. Askan, A. Akinci, and L. Malagnini (2012). Strong-ground-motion simulation of the 6 April 2009 L'Aquila, Italy, earthquake, *Bull. Seismol. Soc. Am.* **102,** 1429–1445.

Wessel, P., and W. H. F. Smith (1998). New, improved version of Generic Mapping Tools released, *Eos Trans. AGU* **79,** no. 47, 579, doi: 10.1029/98EO00426.

Zor, E., E. Sandvol, J. Xie, N. Turkelli, B. Mitchell, A. H. Gasanov, and G. Yetirmishli (2007). Crustal attenuation within the Turkish plateau and surrounding regions, *Bull. Seismol. Soc. Am.* **97,** 151–161.

Istituto Nazionale di Geofisica e Vulcanologia
Via di Vigna Murata 605
00143 Rome, Italy
aybige.akinci@ingv.it
(A.A., L.M.)

Department of Earth and Atmospheric Sciences
Saint Louis University
3642 Lindell Blvd
St. Louis, Missouri 63108
(R.B.H.)

National Earthquake Monitoring Center
Kandilli Observatory and Earthquake Research Institute
Boğaziçi University
34680 Çengelköy, Istanbul, Turkey
(D.K.)

Manuscript received 30 April 2013;
Published Online 20 May 2014